Ensemble Wind Power Prediction Interval with Optimal Reserve Requirement

Hamid Rezaie, Cheuk Hei Chung, and Nima Safari, *Member*, IEEE

Abstract—Wind power prediction interval (WPPI) models in the literature have predominantly been developed for and tested on specific case studies. However, wind behavior and characteristics can vary significantly across regions. Thus, a prediction model that performs well in one case might underperform in another. To address this shortcoming, this paper proposes an ensemble WPPI framework that integrates multiple WPPI models with distinct characteristics to improve robustness. Another important and often overlooked factor is the role of probabilistic wind power prediction (WPP) in quantifying wind power uncertainty, which should be handled by operating reserve. Operating reserve in WPPI frameworks enhances the efficacy of WPP. In this regard, the proposed framework employs a novel bi-layer optimization approach that takes both WPPI quality and reserve requirements into account. Comprehensive analysis with different real-world datasets and various benchmark models validates the quality of the obtained WPPIs while resulting in more optimal reserve requirements.

Index Terms—Ensemble model, linear programming, operating reserve, optimal reserve requirement, prediction interval, probabilistic prediction, renewable integration, uncertainty representation, wind power prediction (WPP).

I. INTRODUCTION

AMID a planetary transformative journey towards net-zero greenhouse gas emissions, power systems have been witnessing an unprecedented level of uncertainty by virtue of the ever-growing penetration of wind power (WP). This calls for versatile wind power prediction (WPP) models to facilitate decision-making in system operation [1].

Probabilistic prediction is an effective tool to represent WP uncertainty, which regards WP as a random variable that can be expressed using different probabilistic measures, including probability density functions (PDFs) and cumulative distribution functions (CDFs), quantiles and intervals, discrete probabilities, and moments of probability distributions, e.g., mean, variance, and skewness. PDFs and CDFs are the most general representation forms and are widely used in stochastic power system optimization problems. Quantiles and prediction intervals (PIs) are the most common and visualized forms, and can predict a range within which the future WP will fall with a specified confidence level (SCL) [2], [3].

Wind power prediction interval (WPPI) models can be classified into two general types: indirect and direct WPPI models. Indirect WPPI models estimate a PDF for WP uncertainty first, according to which the PIs are constructed, whereas direct WPPI models construct WPPIs directly. The PDFs in indirect WPPI models are commonly generated based on the point prediction error for WP utilizing various density estimation (DE) techniques, e.g., [4]-[6]. One drawback of most indirect WPPI models is their limited optimization flexibility in terms of maximizing sharpness while meeting the SCL. This shortcoming is addressed in direct WPPI models. Direct WPPI models are typically optimization-based frameworks that are based on either minimizing or maximizing an objective function associated with WPPI quality-typically by evaluating reliability and PI width. For example, the WPPI models presented in [7] and [8] minimize the PI width while considering reliability as a constraint to meet the SCL. The models in [9]-[16] are based on different objective functions that take both reliability and width measures into account. They minimize PI width and maximize PI reliability at the same time while considering the SCL as the reliability target. Due to the non-differentiability and non-convexity of the cost functions used in [8]-[15], heuristic optimization techniques are utilized. However, heuristic optimization is time-consuming and might result in local optima [17], which led the researchers to come up with linear and/or convex objective functions for WPPI optimization, e.g., [17]-[20].

The WPPI models in the literature have shown rewarding outcomes in the context of WPP. However, a general concern is that they are mainly designed for and tested on certain test cases; yet, WP characteristics vary significantly across regions due to their stochastic nature. As a result, a prediction model that excels when applied to a wind farm with a certain set of features may underperform when applied to another wind farm with a different set of characteristics. To address this shortcoming, this paper proposes a novel ensemble WPPI (EWPPI) framework that is more robust

H. Rezaie (corresponding author) is with the Saskatchewan Power Corporation (SaskPower), Regina, Saskatchewan, Canada (e-mail: h.rezaie@usask.ca).

C. H. Chung is with the Department of Electrical and Computer Engineering and Department of Human Biology, University of Toronto, Toronto, ON M5S 3G4, Canada (e-mail: ch.chung@mail.utoronto.ca).

N. Safari is with the Alberta Electric System Operator (AESO), Calgary, Alberta, Canada (e-mail: n.safari@usask.ca).

against changes in WP characteristics. This framework employs various WPPI models in an integrated structure to simultaneously exploit their advantages. Each WPPI model has an associated weight factor that determines its contribution to the final prediction. The weights of the models are adaptively specified for each test case using a proposed linear optimization to realize the best performance.

In the WPPI literature, most efforts are focused on improving prediction accuracy in terms of broad statistical metrics such as sharpness and reliability level. While these metrics provide helpful information about WPPI quality, the WPPIs still might not be tailored to the operational needs of the power system [21]. Reserve allocation and depletion associated with WP integration could vary based on WPPIs. An emerging trend is toward customizing WPPIs established on operational needs, but this research area is still in its infancy. In [21], a cost-oriented WPPI model based on the extreme learning machine (ELM) is proposed in which the PIs are constructed such that the cost of the regulatory reserve is minimized. In [22], an ELM-based WPPI model is proposed to reduce the total operating reserve costs considering both reserve provision and deficit payments. In the current industry practice, the operating reserve to handle WP uncertainty is calculated based on the deviation of actual WP from the expected WP (i.e., deterministic WPP) [23]-[25]. For reserve definition, it is common to assume a symmetrical interval around the expected WP, the WP point prediction, e.g., using the three-sigma rule for WP error in [23], which is supposed to cover wind uncertainties with the confidence level specified for the operating reserve. It is also quite common for utilities to have both WPPI and deterministic WP products at their disposal. Thus, processing available WPPI and deterministic WP from vendors to consider symmetricity in the final WPPIs with respect to deterministic WPP could provide valuable information about the dynamic reserve requirements (RRs). However, to the best of the authors' knowledge, this has rarely been discussed in the WPPI literature.

The main contributions of this paper are as follows.

1) Developing a novel EWPPI framework to improve prediction robustness. The proposed framework is a straightforward ensemble structure that employs various WPPI models whose contributions to the final WPPI are adaptively determined to maximize performance on any given test system. The ensemble model tuning is realized through an efficient and swift bi-layer optimization technique. The inner layer of the optimization determines the weight of each individual WPPI model via linear programming (LP) with a single hyperparameter obtained from the outer layer. The outer layer is responsible for optimizing the final WPPI while ensuring the SCL is met by adjusting the single hyperparameter, for which it uses a straightforward iterative algorithm with an extremely fast and exponential convergence rate. Notably, the model tuning procedure is entirely independent of the WPPI models employed in the ensemble prediction engine (EPE). Therefore, any WPPI model can be easily integrated into the EPE to further improve performance. Also, due to the independence of the WPPI models within the EPE, parallel processing can be utilized to autonomously and efficiently train these models. As such, the proposed framework does not result in increased computation time.

2) Incorporating RR optimization within the prediction framework. The objective function of the inner layer of model optimization is designed to achieve high-quality WPPIs, which also results in optimized RRs in system operation. This linear objective function determines the optimal ensemble model weights through minimizing PI width, penalizing samples outside of PI, and maximizing PI symmetricity around the deterministic WPP that results in reducing the RR standard deviation as well as the likelihood of high RR values.

The proposed framework will be particularly beneficial for electric utilities and wind farm operators that employ multiple WP forecasts from various vendors to generate a highly accurate final forecast based on the individual forecasts they receive while the RR for handling WP uncertainty is optimized. In the following, Section II describes the overall prediction framework, Section III presents the EPE, Section IV explains the proposed bi-layer optimization approach, Section V evaluates the model's performance, and Section VI presents the conclusions of the paper.

II. Overall Prediction Framework

Figure 1 is an overall schematic diagram of the proposed EWPPI framework. In the proposed framework, the historical WP time series and the associated deterministic WPP are fed into the EPE. In the EPE, various interval-based WPP models from a wide range of prediction methodologies and frameworks are used to construct the candidate WPPIs based on the SCL, which are described in Section III. Then, at the ensemble model optimization stage, the weight associated with the WPPI candidate in the final WPPI is determined through a proposed bi-layer optimization approach.
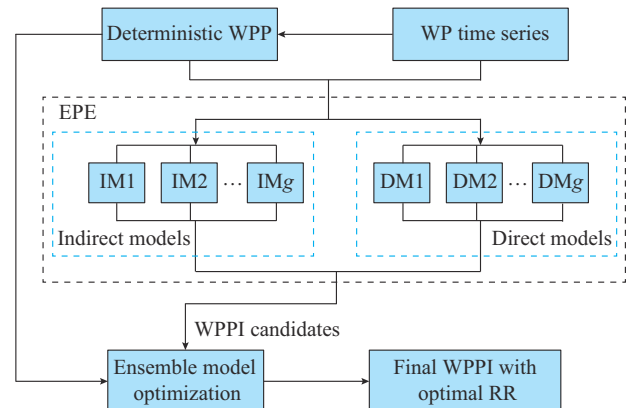
Fig. 1. Schematic diagram of proposed EWPPI framework.

The ensemble weights are optimized based on maximizing WPPI quality (measured based on the PI reliability and sharpness) and maximizing symmetricity with respect to the deterministic WPP that results in a more optimal RR. The bi-layer optimization approach is presented in Section IV.

In Fig. 1, IMj and DMj represent the jth ($j = 1, 2, …, g$) indirect model and direct model, respectively. As observed, the WPPI models are independent, and hence can be implement-

ed using parallel processing. Also, only the output of the models is used at the ensemble model optimization stage, and it is completely independent of the type of WPPI model used. Therefore, any WPPI model can be included in the EPE without requiring any framework modifications. The deterministic prediction model is employed in the proposed framework to also allow for the inclusion of WPPI models based on point prediction error in the EPE.

III. WPPI Candidates

In the proposed framework, a set of indirect and direct WPPI candidates are constructed based on the WP time series and its associated point prediction, each of which is provided by a distinct WPPI model. This section only summarizes the WPPI models used in the numerical experiments (as shown in Section V); however, the proposed EWPPI can utilize the WPPI results from any WPPI model. The WPPI models included in the EPE are categorized in Table I, followed by their description.

TABLE I
WPPI MODELS INCLUDED IN EPE

Type	Category	Model
Indirect	Error-based (parametric)	IM1
	Error-based (non-parametric)	IM2
	Predictive (parametric)	IM3
	Predictive (non-parametric)	IM4
Direct	Error-based	DM1
	Predictive	DM2, DM3, DM4

1) IM1: T location-scale (TLS) DE on point prediction error [4].

2) IM2: kernel DE (KDE) on point prediction error [6].

3) IM3: predictive categorical TLS DE.

4) IM4: predictive categorical KDE.

5) DM1: quantile regression (QR) on point prediction error [4].

6) DM2: predictive categorical QR.

7) DM3: WPPI based on QR and LP without regularization [20].

8) DM4: WPPI based on QR and LP with regularization [18].

Indirect WPPI models first estimate a PDF for WP, and then derive the PI based on that, while direct WPPI models generate PIs directly.

A. Indirect WPPI Models

This subsection explains the process of creating indirect WPPI models included in the EPE.

1) Error-based Indirect WPPI Models

IM1 and IM2 are error-based indirect WPPI models that are developed based on the DE of the WP point prediction error. Then, the PI is constructed by considering a confidence interval around the WP point prediction value. The interval is specified through the following steps.

Step 1: calculate the point prediction error ε_i.

$$\varepsilon_i = T_i - Y_i \quad i = 1, 2, \ldots, N \tag{1}$$

where ε_i is the point prediction error for the ith WP sample; T_i is the target value (actual WP generation) of the ith WP sample; Y_i is the predicted value for the ith WP sample; and N is the total number of WP samples.

Step 2: estimate a PDF for the point prediction error ε. IM1 and IM2 use the TLS distribution (2) and kernel function (3) for DE, respectively.

$$f(\varepsilon; \mu, \sigma, v) = \frac{\Gamma\left(\frac{v+1}{2}\right)}{\sigma \sqrt{v\pi} \, \Gamma\left(\frac{v}{2}\right)} \left[1 + \frac{1}{v}\left(\frac{\varepsilon - \mu}{\sigma}\right)^2\right]^{-\frac{v+1}{2}} \tag{2}$$

$$f_h(\varepsilon) = \frac{1}{Nh} \sum_{i=1}^{N} K\left(\frac{\varepsilon - \varepsilon_i}{h}\right) \tag{3}$$

where μ, σ, and v are the location, scale, and shape parameters, and are chosen to be equal to the mean, standard deviation, and the number of samples in each time window considered for DE, respectively; $\Gamma(\cdot)$ is the Gamma function; $K(\cdot)$ is the kernel function; and $h > 0$ is the smoothing bandwidth. Basically, the kernel density estimator smooths each data point into a small density bump, with these bumps then added together to obtain the final density. Without loss of generalization, the Gaussian kernel (4) is chosen as the kernel function in this paper.

$$K(x) = \frac{1}{\sqrt{2\pi}} e^{-\frac{1}{2}x^2} \tag{4}$$

Step 3: convert the PDF to a CDF and determine the interval according to the CDF and the SCL.

The upper and lower bounds of the interval are equal to the upper and lower quantile values, calculated on the CDF according to the SCL $(1-\alpha)\%$.

For a given SCL $(1-\alpha)\%$, the lower and upper quantiles $(\underline{\alpha}$ and $\bar{\alpha})$ can be determined as:

$$\underline{\alpha} = 1 - \bar{\alpha} = \alpha/2 \tag{5}$$

According to the definition, the value of quantile v (q_v) for a random variable x is the value that satisfies (6):

$$\Pr(x \le q_v) = v \tag{6}$$

Therefore, the value of the lower (upper) quantile $q_{\underline{\alpha}}$ $(q_{\bar{\alpha}})$ is the minimum value whose CDF is greater than or equal to $\underline{\alpha}$ $(\bar{\alpha})$.

Step 4: construct the WPPI by adding the interval to the point prediction result.

$$\begin{cases} \bar{M} = Y + q_{\bar{\alpha}}(\varepsilon) \\ \underline{M} = Y + q_{\underline{\alpha}}(\varepsilon) \end{cases} \tag{7}$$

where $\bar{M}$ and $\underline{M}$ are the upper and lower bounds of the constructed WPPI, respectively; Y is the point prediction result; and $q_{\bar{\alpha}}(\varepsilon)$ and $q_{\underline{\alpha}}(\varepsilon)$ are the upper quantile $\bar{\alpha}$ and lower quantile $\underline{\alpha}$ values calculated from the CDF of ε, respectively.

2) Predictive Indirect WPPI Models

IM3 and IM4 are predictive indirect WPPI models developed based on the DE of the WP time series. These models use a proposed categorical predictive DE approach, in which the WP samples are first divided into several categories, and then a PDF is estimated for each category.

The suggested approach for categorization is based on the slope (SL) of the WP time series in the previous samples, which can be calculated as:

$$SL_i = x_{i-1} - x_{i-2} \tag{8}$$

where SL_i is the SL value for the ith WP sample x_i; and x_{i-1} and x_{i-2} are the WP values in the first and second lags, respectively.

In this approach, the SL value should be first calculated for all samples according to (8). Then, the samples are discretely classified based on their SL value. After categorizing the samples, the difference between each WP sample and its preceding value is calculated as given in (9).

$$\delta_i = x_i - x_{i-1} \tag{9}$$

Next, a PDF is estimated for the δ_i values associated with each category, for which IM3 and IM4 use the TLS distribution (2) and kernel function (3), respectively. These PDFs provide valuable information about WP behavior. Based on these PDFs, the WP value in the following step can be effectively estimated based on the present WP value and its value in the previous step (the slope of the WP time series). In other words, in this differential prediction approach, the model predicts the difference between the current and future WP values based on the difference between the current and prior WP values. After obtaining the PDFs, they should be converted into CDFs, according to which the PIs are determined, as described in *Step 4*.

Overall, considering the aforementioned explanations, to perform WPP at the ith step, first calculate SL_{i+1} using (8) and then determine the category according to SL_{i+1}. Next, specify the upper and lower bounds of the interval according to the category. Finally, construct the WPPI for the next step by adding the specified interval to the current WP value x_i. To perform multi-step prediction using this approach, instead of the actual WP value, its corresponding point prediction value can be used.

B. Direct WPPI Models

This subsection describes the process of creating direct WPPI models included in the EPE.

1) Error-based Direct WPPI Models

DM1 is an error-based direct WPPI model that constructs the WPPI based on the point prediction error directly. DM1 uses the QR technique for PI construction. After calculating the point prediction error $\boldsymbol{\varepsilon} = \begin{bmatrix} \varepsilon_1, \varepsilon_2, \ldots, \varepsilon_N \end{bmatrix}$ according to (1), the objective function given in (10) is used to directly determine the value of the lower and upper quantiles of $\boldsymbol{\varepsilon}$ based on the SCL [18].

$$\min_{\beta_v} \sum_{v \in \{\bar{a}, \underline{a}\}} \sum_{i=1}^{N} \psi_v \left(\varepsilon_i - \xi_v \left(\boldsymbol{E}_i, \beta_v \right) \right) \tag{10a}$$

$$\psi_v(x) = \begin{cases} vx & x \geq 0 \\ (v-1)x & x < 0 \end{cases} \tag{10b}$$

$$\boldsymbol{E}_i = \begin{bmatrix} \varepsilon_{i-d} & \varepsilon_{i-d-1} & \ldots & \varepsilon_{i-1} \end{bmatrix} \tag{10c}$$

where β_v denotes the unknown parameters of the QR function $\xi_v \left(\boldsymbol{E}_i, \beta_v \right)$ associated with the vth quantile; $\psi_v(\cdot)$ is an absolute value linear penalty function; and d is the number of

lags used as the input to $\xi_v \left(\boldsymbol{E}_i, \beta_v \right)$. $\xi_v \left(\boldsymbol{E}_i, \beta_v \right)$ can be linearly formulated based on a linear regression or ELM. As $\psi_v(\cdot)$ and $\xi_v \left(\boldsymbol{E}_i, \beta_v \right)$ are linear, the resulting optimization problem forms an LP. After calculating the upper quantile value $q_{\bar{a}}(\varepsilon)$ and the lower quantile value $q_{\underline{a}}(\varepsilon)$ using (10), the WPPI is constructed according to (7).

2) Predictive Direct WPPI Models

DM2, DM3, and DM4 are predictive direct WPPI models that directly construct the WPPI based on the WP time series. DM2 uses a categorical predictive DE approach similar to that described for the predictive indirect models in the previous subsection. The difference between DM2 and the predictive indirect WPPI models is that DM2 does not require PDF estimation prior to PI construction. Instead, it uses the QR technique (10) to directly determine the PI (the upper and lower quantile values) for each category. DM3 [20] and DM4 [18] use two different objective functions for WPPI construction, both of which are convex, developed based on QR, and solved using LP.

IV. PROPOSED BI-LAYER OPTIMIZATION APPROACH

This section describes the proposed bi-layer optimization approach to tuning the ensemble model and optimizing the WPPI.

A. Inner Layer Optimization

The inner layer optimization determines the ensemble weights to maximize the WPPI quality. A novel linear objective function is designed for this layer. Assume the EPE consists of m distinct WPPI models. Then, the final WPPI can be obtained from (11).

$$\begin{cases} \bar{y}_i = \bar{\boldsymbol{a}}^{\mathrm{T}} \bar{\boldsymbol{M}}_i \\ \underline{y}_i = \underline{\boldsymbol{a}}^{\mathrm{T}} \underline{\boldsymbol{M}}_i \end{cases} \tag{11}$$

where $\bar{y}_i$ and $\underline{y}_i$ are the final upper and lower bounds predicted for the ith WP sample, respectively; $\bar{\boldsymbol{a}}$ and $\underline{\boldsymbol{a}}$ are the $M \times 1$ vectors containing the weight of WPPI candidates associated with the upper and lower bounds, respectively, and M is the total number of WPPI candidates; and $\bar{\boldsymbol{M}}_i$ and $\underline{\boldsymbol{M}}_i$ are the $M \times 1$ vectors consisting of the upper and lower bounds predicted by the M models for the ith WP sample, respectively.

The objective function given in (12) is proposed to determine the ensemble weights, i. e., the contribution of each WPPI model to the final WPPI. This objective function is designed to maximize WPPI quality by minimizing the width of the PIs while penalizing samples outside of the intervals and attempting to construct symmetric intervals around the WP point prediction. The L1 regularization (Lasso regression) of the ensemble weights is also considered in (12) to prevent overfitting.

$$\min_{\bar{\boldsymbol{a}}, \underline{\boldsymbol{a}}} \sum_{i=1}^{N} \left(W(U_i) + W(L_i) + k_s \left| \hat{U}_i - \hat{L}_i \right| \right) + k_r \left(\| \bar{\boldsymbol{a}} \|_1 + \| \underline{\boldsymbol{a}} \|_1 \right) \tag{12a}$$

$$W(x) = \begin{cases} x & x \geq 0 \\ -x \cdot PF & x < 0 \end{cases} \tag{12b}$$

$$\begin{cases} U_i = \bar{y}_i - T_i \\ L_i = T_i - \underline{y}_i \end{cases} \quad i = 1, 2, \ldots, N \qquad (12c)$$

$$\begin{cases} \hat{U}_i = \bar{y}_i - Y_i \\ \hat{L}_i = Y_i - \underline{y}_i \end{cases} \quad i = 1, 2, \ldots, N \qquad (12d)$$

where i is the sample number; $PF \geq 1$ is the penalty factor for the samples located outside of the final interval; T_i and Y_i are the actual and predicted WP values associated with the ith sample, respectively; and $k_s \geq 0$ and $k_r \geq 0$ are the symmetricity and regularization importance parameters, respectively.

By defining variables $\bar{y}$, $\underline{y}$, γ^{sym}, $\bar{\gamma}^{reg}$, and $\underline{\gamma}^{reg}$, (12) can be converted into an LP model, as given in (13).

$$\min_{S} \left[\sum_{i=1}^{N} \left(\bar{y}_i + \underline{y}_i + \gamma_i^{sym} \right) + \sum_{j=1}^{M} \left(\bar{\gamma}_j^{reg} + \underline{\gamma}_j^{reg} \right) \right] \qquad (13a)$$

s.t.

$$\bar{y}_i \geq U_i \geq -\bar{y}_i / PF \quad i = 1, 2, \ldots, N \qquad (13b)$$

$$\underline{y}_i \geq L_i \geq -\underline{y}_i / PF \quad i = 1, 2, \ldots, N \qquad (13c)$$

$$\gamma_i^{sym} \geq k_s \left(\hat{U}_i - \hat{L}_i \right) \geq -\gamma_i^{sym} \quad i = 1, 2, \ldots, N \qquad (13d)$$

$$\bar{\gamma}_j^{reg} \geq k_r \bar{a}_j \geq -\bar{\gamma}_j^{reg} \quad j = 1, 2, \ldots, M \qquad (13e)$$

$$\underline{\gamma}_j^{reg} \geq k_r \underline{a}_j \geq -\underline{\gamma}_j^{reg} \quad j = 1, 2, \ldots, M \qquad (13f)$$

$$\bar{a}_j, \underline{a}_j, \bar{\gamma}_j^{reg}, \underline{\gamma}_j^{reg} \geq 0 \quad j = 1, 2, \ldots, M \qquad (13g)$$

$$\bar{y}_i, \underline{y}_i, \gamma_i^{sym} \geq 0 \quad i = 1, 2, \ldots, N \qquad (13h)$$

where $S = \left\{ \bar{a}, \underline{a}, \bar{y}, \underline{y}, \gamma^{sym}, \bar{\gamma}^{reg}, \underline{\gamma}^{reg} \right\}$.

This linear optimization problem (13) is solved based on a pre-determined PF value, which is optimally set by the outer layer, as elucidated in Section IV-C. In the following, the objective function in (13) and its associated constraints are further explicated.

The cost function in (13a) is comprised of two summation terms. The first ensures high-quality PIs with symmetricity consideration, while the second ensures a robust model and alleviates the risk of overfitting. In the first term, $\bar{y}_i$ and $\underline{y}_i$ penalize the ensemble model if the upper or lower bounds of the PI deviate from sample point (T_i). Penalties corresponding to $\bar{y}_i$ and $\underline{y}_i$ are determined based on (13b) and (13c), respectively. A higher PF results in larger penalties when the upper bound ($\bar{y}_i$) or lower bound ($\underline{y}_i$) is less than or larger than the sample point (T_i), respectively. γ_i^{sym} in (13a) penalizes the PIs that are asymmetric with respect to the deterministic forecast (Y_i). The minimum γ_i^{sym} is determined such that (13d) holds. k_s in (13d) is a user-defined hyperparameter that determines the importance of symmetricity. Formulas (13e) and (13f) are associated with regularization terms in the cost function to cope with over-training.

B. Optimal RR

This subsection describes how constructing symmetric in-

tervals around the expected WP value, i.e., minimizing γ^{sym} in (13), can result in optimal RRs.

In the current industry practice, operating reserve to handle WP uncertainty is typically calculated based on the deviation of actual WP from the dispatched level, while WP is dispatched at the expected values obtained from deterministic forecasts. An interval is considered around the expected WP, i.e., the WP point prediction, which is supposed to cover wind uncertainties with the confidence level specified for the operating reserve. For instance, the three-sigma rule (i.e., confidence level of 99.7%) is applied to the WPP error to determine the regulating RR associated with WP uncertainty in the Eastern Wind Integration and Transmission Study [23], [26]. In [24], the imbalance RR is defined based on hour-ahead deterministic forecast error. Having both deterministic WPP and WPPI to determine the RR for each time interval, the difference between the lower and upper bounds of the WPPI and the WP point prediction can be considered as the ramp-up reserve (RUR) and ramp-down reserve (RDR) requirements, respectively. In other words, WPPIs represent the potential overestimation and underestimation of the WP, which should be compensated for by the RUR and RDR, respectively.

Unlike conventional WPPIs that do not take RR into account and could be irrelevant to the WP point prediction, the proposed approach constructs the PIs tending to center the WP point prediction. Therefore, the proposed WPPI results in less variation in RUR and RDR requirements from one time interval to another. This lower variation facilitates decision-making in real-time power system operation, as operators do not expect significant changes in RUR and RDR in different time intervals. It also reduces the likelihood of high RR values for wind uncertainty, which improves economic operation and enhances system reliability when the available reserve is limited. Figure 2 is a simplified illustration of the prior statements, where L can be any positive values ($\mathbb{R}^+$). Without taking symmetricity into account, note that RDR is high when RUR is low, and vice versa.
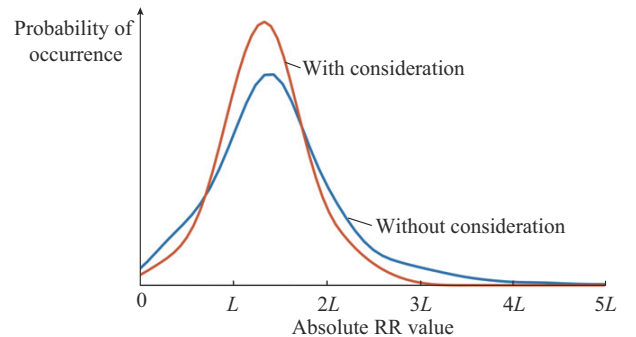
Fig. 2. Empirical PDF of absolute RR value with and without consideration of interval symmetricity around WP point prediction.

C. Outer Layer Optimization

The outer layer is responsible for optimizing the reliability and sharpness of the final WPPI. A straightforward algorithm is designed that optimizes the WPPI using a single control variable: the PF value used in the inner layer (13).

Figure 3 is a flowchart of the proposed algorithm.
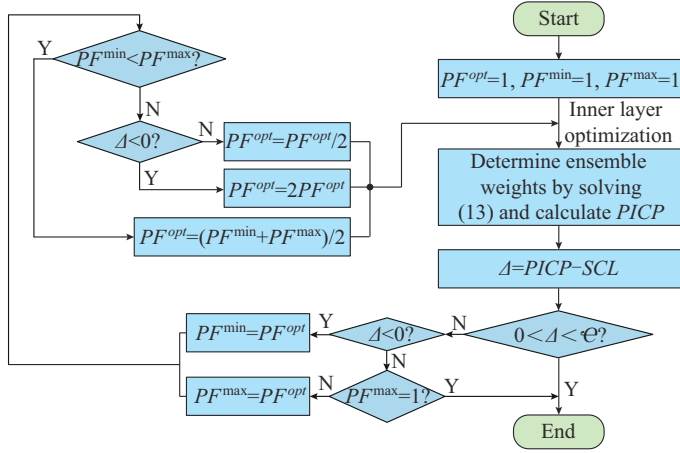
Fig. 3.   Outer layer optimization determining optimal PF.

In Fig. 3, the PI coverage probability (PICP) measures the PI reliability and is calculated using (14), considering the SCL that must be satisfied. $\mathcal{C}$ determines the maximum acceptable positive deviation from the SCL, which is 1% in this paper.

$$PICP = \frac{1}{N_T}\sum_{i=1}^{N_T}\theta_i \times 100\% \qquad (14a)$$

$$\theta_i = \begin{cases} 1 & \underline{y}_i \leq T_i \leq \bar{y}_i \\ 0 & \text{otherwise} \end{cases} \qquad (14b)$$

where N_T is the total number of test WP samples. The proposed algorithm begins with an initial value (PF^0) for the optimal PF (PF^{opt}). Then, according to Fig. 3, it finds two PF values: one lower than the actual PF^{opt} called PF^{min}, and the other higher than the actual PF^{opt} called PF^{max}. On the one hand, solving (13) based on PF^{min} results in PIs that are too sharp and consequently unable to meet the SCL. On the other hand, solving (13) based on PF^{max} results in PIs that are excessively wider than necessary to satisfy the SCL. Thereafter, the algorithm considers the mean of PF^{max} and PF^{min} as the new PF^{opt}. If solving (13) based on this PF^{opt} results in a PICP value lower than the SCL, this PF value is considered the new PF^{min}; likewise, if the calculated PICP is higher than the $SCL + \mathcal{C}$, it is considered the new PF^{max}. Then, PF^{opt} is set equal to the mean of the updated values of PF^{max} and PF^{min}, and this procedure is repeated until the actual PF^{opt} is found. The actual PF^{opt} is the PF value that results in a PICP value greater than the SCL and lower than $SCL + \mathcal{C}$.

Because the proposed algorithm approaches PF^{opt} by the power of 2, it has an extremely fast convergence rate and requires only a few iterations to reach the optimal solution. This algorithm adjusts the model's PICP according to its reference value (SCL) and results in WPPIs that are optimal in terms of both reliability and sharpness. The PI sharpness has an inverse relationship with the PF; increasing the PF results in increasing the PI width to decrease the number of samples located outside of the interval. Therefore, the proposed algorithm optimizes the sharpness by adjusting the PF

while considering the reliability (PICP) as a constraint. This constraint also ensures optimum reliability by preventing the construction of PIs with insufficient or excessive PICP values.

To summarize the proposed bi-layer optimization approach, it follows an iterative optimization process. Within each iteration, the outer layer assigns a value to the hyper-parameter PF. Subsequently, the inner layer performs optimization of ensemble weights, according to (13), to minimize the width of the final WPPI. Upon attainment of these optimized ensemble weights, the PICP is computed, which is then employed by the outer layer to adaptively update the PF value, according to Fig. 3. The termination criterion for this iterative procedure is met when the calculated PICP surpasses the SCL, ensuring the fulfillment of the reliability target, while also remaining below the threshold of $SCL + \mathcal{C}$ to prevent the emergence of excessively wide PIs.

V. NUMERICAL RESULTS AND DISCUSSIONS

A. Test Systems, Evaluation Factors, and Model Tuning

This subsection evaluates the effectiveness of the proposed EWPPI framework using three real-world WP generation datasets. Case 1 (ALB) features historical WP generation data from Alberta, Canada, for December 2014 to December 2015 [27]. Case 2 (CEN) features historical WP generation data from Centennial wind farm in Saskatchewan, Canada, for December 2014 to December 2015, provided by SaskPower. Case 3 (SOT) features historical WP generation data from Sotavento wind farm, Spain, for December 2019 to December 2020 [28]. The time resolution of all datasets is 10 min. The performance of the WPPI models is assessed using the evaluation factors given in (14)-(18) [9], [12], [15].

$$PIAW = \frac{1}{N_T}\sum_{i=1}^{N_T}\left(\bar{y}_i - \underline{y}_i\right) \times 100\% \qquad (15)$$

$$CWC = PIAW \cdot \left(1 + Qe^{-\mathcal{V}(PICP-SCL)}\right) \times 100\% \qquad (16a)$$

$$Q = \begin{cases} 0 & PICP \geq SCL \\ 1 & PICP < SCL \end{cases} \qquad (16b)$$

$$PIOS = \frac{1}{N_T}\left|\sum_{i=1}^{N_T}Sc_i\right| \times 100\% \qquad (17a)$$

$$Sc_i = \begin{cases} -2\alpha\left(\bar{y}_i - \underline{y}_i\right) - 4\left(\underline{y}_i - T_i\right) & T_i < Y_i^l \\ -2\alpha\left(\bar{y}_i - \underline{y}_i\right) - 4\left(T_i - \bar{y}_i\right) & T_i > Y_i^u \\ -2\alpha\left(\bar{y}_i - \underline{y}_i\right) & \text{otherwise} \end{cases} \qquad (17b)$$

$$ACS = \frac{1}{N_{case}}\sum_{j=1}^{N_{case}}Q_j\left(SCL_j - PICP_j\right) \qquad (18)$$

where N_{case} is the number of cases for which the WPPIs are constructed; and $\mathcal{V}$ is a kind of penalty factor dissatisfying the SCL, which is chosen to be 50 according to [15].

The model is re-trained every three days using the most recent 30-day data. The symmetricity (k_s) and regularization (k_r) importance parameters are considered to be 10 and 0.01,

respectively. For all WPPI models implemented in this paper, the number of hidden neurons (NHN) and the input vector dimension (IVD) (the number of previous time steps considered as input) for each case are optimally set and updated monthly using the five-fold cross-validation technique [29]. A three-layer loop is defined to implement the five-fold cross-validation technique, shown in the following pseudocode.

Pseudocode of the five-fold cross-validation technique

for $IVD = 2:12$
  for $NHN = 5:5:60$
    for $K = 1:5$
      Train the model using the training data
      $PIOS(K) \leftarrow$ Calculate *PIOS* on the validation data
    end
    $CV(IVD, NHN) = mean(PIOS)$
  end
end

The five-fold cross-validation results in an 11×12 matrix with the cell with the lowest value determining the best IVD and NHN values. Due to the enormous number of simulations needed to implement the five-fold cross validation approach as well as the low variability of NHN and IVD over short time periods, cross validation was only applied monthly; hence, IVD and NHN are optimized at the beginning of each month.

B. WPPIs: Overall Performance

The effectiveness of the proposed EWPPI framework is evaluated through comparison with the following benchmarks.

BM1: the direct WPPI model based on QR and LP, without regularization, presented in [20].

BM2: the direct WPPI model based on QR and LP, with regularization, presented in [18].

BM3: the lower upper bound estimation method presented in [8], which optimizes the WPPI by minimizing the PI average width (PIAW) (15) while considering PICP as a constraint.

BM4: the lower upper bound estimation method presented in [15], which optimizes the WPPI by minimizing the coverage width-based criterion (CWC) (16).

BM5: the lower upper bound estimation method presented in [12], which optimizes the WPPI by minimizing the PI overall score (PIOS) (17).

Note that BM1 and BM2 are included in the EPE as DM3 and DM4, respectively. To evaluate the WPPI models, their performance is simulated for one year with two different forecast horizons: 30-min and 1-hour ahead. The WPPIs are constructed based on SCLs of 90% and 95%, as WPP with high confidence levels is required in practice to ensure reliable and optimal operation of power systems. The detailed results obtained from the WPPI models are presented in Tables II-V.

According to Tables II-IV, the models based on QR (BM1 and BM2) provide the sharpest WPPIs on average compared with the other WPPI models. However, they are unable to achieve sufficient PICP values to satisfy the SCL for the pre-

diction. Among the three other benchmarks (BM3, BM4, and BM5), BM5 is more successful in terms of meeting the SCL and results in WPPIs with lower CWC and PIOS values. The model training procedure for these three models requires heuristic optimization, which is significantly more time-consuming than the training procedure for QR-based models and the proposed EWPPI implemented in this paper.

TABLE II
PERFORMANCE EVALUATION OF WPPI MODELS FOR CASE 1 (ALB)

SCL (%)	Forecast horizon	Model	PICP (%)	PIAW (%)	CWC (%)	PIOS (%)
90	30-min	BM1	88.49	6.35	19.88	2.20
		BM2	89.46	6.50	15.01	2.24
		BM3	89.63	11.09	24.45	3.25
		BM4	90.25	10.89	10.89	3.12
		BM5	89.69	11.09	24.03	3.10
		EWPPI	90.12	7.20	7.20	2.14
	1-hour	BM1	89.02	10.56	27.80	3.38
		BM2	89.44	10.39	24.15	3.50
		BM3	88.98	15.43	41.09	4.58
		BM4	89.20	14.83	36.98	4.31
		BM5	90.07	15.47	15.47	4.34
		EWPPI	90.59	11.33	11.33	3.14
95	30-min	BM1	93.66	8.20	24.26	1.44
		BM2	94.28	8.47	20.59	1.38
		BM3	94.63	13.58	29.92	1.90
		BM4	94.31	13.86	33.46	1.94
		BM5	95.56	13.81	13.81	1.79
		EWPPI	95.29	10.02	10.02	1.30
	1-hour	BM1	94.25	13.56	33.29	2.12
		BM2	93.83	13.52	37.76	2.18
		BM3	94.02	17.85	46.96	2.57
		BM4	94.09	18.26	47.11	2.59
		BM5	94.29	18.61	45.16	2.48
		EWPPI	95.41	15.92	15.92	2.00

These results demonstrate the superiority of the proposed EWPPI framework over the benchmark models as well as the robustness and flexibility of its performance. According to the results, the proposed EWPPI framework performs better than the convex WPPI models (BM1 and BM2) by 57.49% in terms of the average CWC, 11.57% in terms of the average PIOS, and 100% in terms of the average coverage shortage (ACS). It also outperforms the non-convex WPPI models (BM3, BM4, and BM5) by 57.47% in terms of the average CWC, 18.31% in terms of the average PIOS, and 100% in terms of the ACS.

According to Tables II-IV, the proposed EWPPI framework is the most proficient model among all WPPI models in terms of satisfying the SCL requirement. Compared with the five benchmark models, EWPPI provides the sharpest PIs while meeting the SCL, and its CWC and PIOS values are the lowest among all prediction models for all case studies. In terms of all evaluation factors presented in Table V, EWPPI outperforms all other models.

TABLE III
PERFORMANCE EVALUATION OF WPPI MODELS FOR CASE 2 (CEN)

SCL (%)	Forecast horizon	Model	PICP (%)	PIAW (%)	CWC (%)	PIOS (%)
90	30-min	BM1	89.37	15.69	37.15	5.68
		BM2	89.80	15.39	32.42	5.80
		BM3	89.74	19.73	42.25	6.35
		BM4	89.89	19.30	39.65	6.24
		BM5	90.72	20.02	20.02	5.85
		EWPPI	90.92	16.73	16.73	4.96
	1-hour	BM1	89.22	23.24	57.52	7.87
		BM2	88.64	21.52	63.99	8.13
		BM3	89.44	25.22	58.63	7.94
		BM4	89.03	24.97	65.49	8.06
		BM5	90.00	26.57	53.21	7.56
		EWPPI	90.43	24.30	24.30	6.91
95	30-min	BM1	94.23	20.94	51.79	3.57
		BM2	94.76	21.08	44.87	3.70
		BM3	94.55	25.06	56.48	3.83
		BM4	94.62	25.21	55.64	3.82
		BM5	95.19	25.31	25.31	3.54
		EWPPI	95.37	23.97	23.97	3.32
	1-hour	BM1	94.35	31.02	73.91	4.90
		BM2	93.12	28.79	102.37	5.35
		BM3	94.21	32.09	79.66	4.84
		BM4	94.06	31.94	83.05	4.90
		BM5	94.86	33.92	70.33	4.53
		EWPPI	95.55	32.85	32.85	4.34

TABLE IV
PERFORMANCE EVALUATION OF WPPI MODELS FOR CASE 3 (SOT)

SCL (%)	Forecast horizon	Model	PICP (%)	PIAW (%)	CWC (%)	PIOS (%)
90	30-min	BM1	88.95	11.87	31.97	4.27
		BM2	89.67	11.84	25.78	4.40
		BM3	89.75	16.21	34.62	5.15
		BM4	89.98	16.01	32.14	5.05
		BM5	90.27	16.55	16.55	4.75
		EWPPI	90.65	12.89	12.89	3.81
	1-hour	BM1	89.11	18.16	46.49	6.01
		BM2	88.87	17.06	47.07	6.28
		BM3	89.18	21.29	53.44	6.64
		BM4	89.13	20.84	53.08	6.51
		BM5	90.12	22.21	22.21	6.37
		EWPPI	90.51	19.17	19.17	5.50
95	30-min	BM1	94.02	15.91	41.86	2.72
		BM2	94.65	16.05	35.18	2.84
		BM3	94.50	20.39	46.54	3.07
		BM4	94.60	20.60	45.81	3.14
		BM5	95.38	20.80	20.80	2.90
		EWPPI	95.28	18.50	18.50	2.47
	1-hour	BM1	94.21	24.13	59.94	3.71
		BM2	93.34	22.69	74.63	4.05
		BM3	94.09	26.40	67.94	3.94
		BM4	94.01	26.37	69.58	3.99
		BM5	94.59	27.85	61.99	3.80
		EWPPI	95.42	26.01	26.01	3.35

C. WPPIs: Seasonal Performance

The seasonal performance of the WPPI models is also investigated for 1-hour ahead prediction with an SCL of 90% to evaluate the model performance in greater detail. The results obtained from this analysis are presented in Tables VI-IX.

According to results presented in Tables VI-IX, the proposed framework is capable of consistently generating high-quality PIs despite the seasonal variations in wind characteristics. Among all WPPI models implemented, EWPPI is the most reliable and efficient model, being considerably more successful in satisfying the SCL over different seasons while generating sharp WPPIs. The average CWC, average PIOS, and ACS values for the PIs constructed by EWPPI are the lowest of all models for all case studies. The seasonal performance evaluation results demonstrate the high robustness of the proposed EWPPI framework to variations in wind characteristics.

In regard to the optimization problems defined for WPPI construction in the benchmark models, BM2, BM3, and BM4 use non-convex objective functions that should be solved using heuristic algorithms, which are time-consuming and not as reliable as they might get trapped into local optima. BM1 and BM2 are based on convex objective functions, so they can be efficiently solved with a global solution.

However, the solutions obtained using these models are only the best solutions for the defined cost function, not necessarily the best WPPI. In other words, these convex models construct the best WPPI based on QR, not the best WPPI that could be constructed. As the numerical results show, the intervals constructed based on QR are usually too sharp, and their quality drastically decreases as the prediction horizon increases.

D. Impact of Symmetricity on RR

This subsection investigates the impact of the symmetricity factor on RR and PI quality. The 1-hour ahead WPPI for Case 1 (ALB) with an SCL of 90% is considered for analysis as an example. To evaluate the PI symmetricity around the WP point prediction, two symmetricity measures, $SM1$ and $SM2$, are defined as given in (19) and (20), respectively. The lower the $SM1$ and $SM2$ values, the more symmetric the WPPI; for a perfectly symmetric PI, $SM1$ and $SM2$ both equal zero ($\hat{U}_i = \hat{L}_i, i = 1, 2, ..., N_T$).

$$SM1 = \frac{1}{N_T} \sum_{i=1}^{N_T} \left| \hat{U}_i - \hat{L}_i \right| \times 100\% \tag{19}$$

$$SM2 = \sqrt{\frac{1}{N_T} \sum_{i=1}^{N_T} \left(\hat{U}_i - \hat{L}_i \right)^2} \times 100\% \tag{20}$$

TABLE V
AVERAGE VALUES OF EVALUATION FACTORS

Case	Model	Average CWC (%)	Average PIOS (%)	ACS (%)
ALB	BM1	26.31	2.29	1.15
	BM2	24.38	2.33	0.75
	BM3	35.61	3.08	0.69
	BM4	32.11	2.99	0.60
	BM5	24.62	2.93	0.25
	EWPPI	11.12	2.15	0.00
CEN	BM1	55.09	5.51	0.71
	BM2	60.91	5.75	0.92
	BM3	59.26	5.74	0.52
	BM4	60.96	5.76	0.60
	BM5	42.22	5.37	0.04
	EWPPI	24.46	4.88	0.00
SOT	BM1	45.07	4.18	0.93
	BM2	45.67	4.39	0.87
	BM3	50.64	4.70	0.62
	BM4	50.15	4.67	0.57
	BM5	30.39	4.46	0.10
	EWPPI	19.14	3.78	0.00

TABLE VI
SEASONAL PERFORMANCE EVALUATION OF MODELS FOR CASE 1 (ALB)

Season	Model	PICP (%)	PIAW (%)	CWC (%)	PIOS (%)
Winter	BM1	89.51	10.34	23.55	3.19
	BM2	89.98	10.29	20.68	3.34
	BM3	89.26	14.86	36.37	4.50
	BM4	89.38	14.15	33.44	4.23
	BM5	91.81	14.68	14.68	4.15
	EWPPI	90.94	10.87	10.87	3.03
Spring	BM1	88.77	10.47	29.84	3.33
	BM2	89.41	10.00	23.43	3.39
	BM3	88.72	15.36	44.49	4.45
	BM4	89.37	15.47	36.67	4.38
	BM5	88.86	16.08	44.51	4.48
	EWPPI	90.76	11.04	11.04	3.00
Summer	BM1	88.53	10.28	31.72	3.56
	BM2	89.32	10.03	24.12	3.74
	BM3	88.77	13.99	39.87	4.54
	BM4	88.77	13.70	39.04	4.24
	BM5	89.04	14.50	37.93	4.35
	EWPPI	90.29	11.68	11.68	3.42
Autumn	BM1	89.28	11.15	27.13	3.45
	BM2	89.04	11.24	29.40	3.51
	BM3	89.18	17.50	43.87	4.85
	BM4	89.28	15.97	38.86	4.41
	BM5	90.58	16.60	16.60	4.38
	EWPPI	90.38	11.72	11.72	3.10

TABLE VII
SEASONAL PERFORMANCE EVALUATION OF MODELS FOR CASE 2 (CEN)

Season	Model	PICP (%)	PIAW (%)	CWC (%)	PIOS (%)
Winter	BM1	90.18	22.51	22.51	7.08
	BM2	89.43	20.66	48.13	7.04
	BM3	90.53	24.84	24.84	7.32
	BM4	90.67	24.51	24.51	7.09
	BM5	91.18	24.94	24.94	6.85
	EWPPI	90.49	22.96	22.96	6.34
Spring	BM1	88.35	22.87	75.06	7.53
	BM2	88.16	20.60	72.29	8.06
	BM3	90.16	24.83	24.83	7.56
	BM4	87.88	24.31	94.48	7.97
	BM5	89.88	25.71	53.01	7.30
	EWPPI	91.20	22.78	22.78	6.88
Summer	BM1	89.28	23.01	55.99	8.56
	BM2	88.21	21.57	74.36	8.90
	BM3	89.23	25.80	63.72	8.60
	BM4	89.14	24.03	60.97	8.49
	BM5	89.42	26.53	61.99	7.90
	EWPPI	89.81	28.39	59.61	7.65
Autumn	BM1	89.09	24.56	63.27	8.33
	BM2	88.77	23.22	66.17	8.50
	BM3	87.84	25.40	100.19	8.29
	BM4	88.44	27.04	86.03	8.68
	BM5	89.51	29.09	66.26	8.21
	EWPPI	90.24	22.97	22.97	6.75

$$RR = RUR \bigcup RDR \tag{21a}$$

$$RUR = \begin{cases} \hat{U}_i & \hat{U}_i > 0 \\ 0 & \hat{U}_i \leq 0 \end{cases} \quad i = 1, 2, \ldots, N_T \tag{21b}$$

$$RDR = \begin{cases} \hat{L}_i & \hat{L}_i > 0 \\ 0 & \hat{L}_i \leq 0 \end{cases} \quad i = 1, 2, \ldots, N_T \tag{21c}$$

As expected, the results indicate increasing k_s decreases both $SM1$ and $SM2$, which leads to a decrease in the standard deviation of RR. Note that k_s shall not be set to excessively high values, otherwise, it will result in unstable outcomes as shown in Table X for $k_s = 100$. It is worth mentioning that as demonstrated in Table X, in addition to the standard deviation, the average RR can also decrease as k_s increases. Taking symmetricity into account in WPPI optimization using the proposed objective function does not degrade PI quality but rather improves it. In other words, PI quality does not need to be compromised in exchange for a lower RR. The PIOS values in Table X indicate the proposed framework reduces the RR while also improving the PI quality.

To visualize the RR distribution, a violin plot of the RR is given in Fig. 4, representing the swarm scatter plot and the corresponding boxplot for three different k_s values with $k_r = 0.01$. According to Fig. 4, increasing the symmetricity importance factor (k_s) in the WPPI optimization increases the RR density around a median value, reducing the probability of the occurrence of high RR values.

The results of the WPPI construction with different k_r and k_s values for the specified test system are given in Table X, where the RR is calculated as:

TABLE VIII
SEASONAL PERFORMANCE EVALUATION OF MODELS FOR CASE 3 (SOT)

Season	Model	PICP (%)	PIAW (%)	CWC (%)	PIOS (%)
Winter	BM1	89.88	17.63	36.39	5.38
	BM2	89.63	16.53	36.46	5.52
	BM3	89.95	20.80	42.15	6.15
	BM4	90.17	20.36	20.36	5.88
	BM5	91.44	20.99	20.99	5.84
	EWPPI	90.52	18.21	18.21	5.16
Spring	BM1	88.52	17.94	55.51	5.83
	BM2	88.56	16.30	49.84	6.18
	BM3	89.53	21.02	47.62	6.30
	BM4	88.52	20.66	63.86	6.47
	BM5	89.49	21.90	50.11	6.27
	EWPPI	90.95	18.14	18.14	5.33
Summer	BM1	88.85	17.95	49.78	6.41
	BM2	88.48	16.91	53.04	6.85
	BM3	88.95	21.06	56.65	7.09
	BM4	89.02	19.76	52.02	6.81
	BM5	89.46	21.73	50.20	6.63
	EWPPI	90.17	21.76	21.76	6.04
Autumn	Model	89.19	19.12	47.81	6.42
	BM1	88.82	18.50	51.96	6.57
	BM2	88.29	22.28	74.62	7.02
	BM3	88.80	22.58	63.65	6.88
	BM4	90.08	24.21	24.21	6.75
	BM5	90.42	18.49	18.49	5.47

TABLE IX
AVERAGE VALUES OF EVALUATION FACTORS FOR SEASONAL PERFORMANCE

Case	Model	Average CWC (%)	Average PIOS (%)	ACS (%)
ALB	BM1	28.06	3.38	0.98
	BM2	24.41	3.50	0.56
	BM3	41.15	4.59	1.02
	BM4	37.00	4.32	0.80
	BM5	28.43	4.34	0.52
	EWPPI	11.33	3.14	0.00
CEN	BM1	54.21	7.88	0.82
	BM2	65.24	8.13	1.36
	BM3	53.40	7.94	0.73
	BM4	66.50	8.06	1.14
	BM5	51.55	7.57	0.30
	EWPPI	32.08	6.91	0.05
SOT	BM1	47.37	6.01	0.89
	BM2	47.82	6.28	1.13
	BM3	55.26	6.64	0.82
	BM4	49.97	6.51	0.91
	BM5	36.38	6.37	0.26
	EWPPI	19.15	5.50	0.00

For instance, in this test system and for three k_s values of 0, 0.1, and 10, the probability of having an RR greater than 100 MW is 23.0%, 17.6%, and 10.3%, respectively. This probability for RR values greater than 150 MW is 5.8%, 2.1%, 0.7%, respectively, implying the likelihood of RR values greater than 150 MW with $k_s = 0$ is over 8 times greater than that with $k_s = 10$.

TABLE X
PERFORMANCE RESULTS WITH DIFFERENT k_r AND k_s VALUES

| k_r	k_s	PIOS (%)	SM1 (%)	SM2 (%)	RR (MW) Mean	RR (MW) Standard deviation
0.00	0.00	3.31	2.10	2.99	77	43
	0.01	3.28	2.08	2.88	79	40
	0.10	3.34	2.00	2.75	78	39
	1.00	3.22	1.32	1.78	74	32
	10.00	3.17	1.27	1.60	70	28
	100.00	3.64	1.30	1.66	76	39
0.01	0.00	3.30	2.14	3.01	78	42
	0.01	3.33	2.11	2.82	79	41
	0.10	3.32	1.87	2.81	76	32
	1.00	3.21	1.36	1.79	72	30
	10.00	3.14	1.17	1.47	69	26
	100.00	3.65	1.45	1.95	77	35
0.10	0.00	3.35	2.26	3.04	78	43
	0.01	3.32	2.09	2.88	77	42
	0.10	3.23	1.82	2.49	75	34
	1.00	3.19	1.34	1.84	73	29
	10.00	3.14	1.19	1.55	69	27
	100.00	4.11	1.42	2.03	79	41
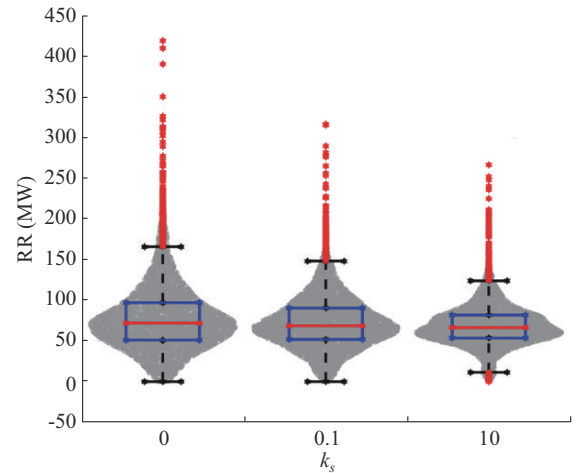
Fig. 4. Impact of k_s on RR.

According to the numerical results presented in this section, the proposed framework can improve the WPPI robustness and optimize the operating reserve required to cover the WPP error. It alleviates RR variations and reduces the likelihood of high RRs. Reducing the RR for wind uncertainty not only makes system operation more economical but also boosts system reliability in time frames when the system capacity is limited, as it allows for more operating reserve to be considered for other uncertain system parameters such as

load, solar, and interchange.

VI. CONCLUSION

This paper introduced a novel EWPPI framework with the goal of improving prediction robustness to variations in wind characteristics and realizing a more optimal RR allocated to cover wind uncertainty. By integrating various WPPI models with distinct characteristics, the proposed framework is proficient in terms of constructing high-quality WPPIs for a variety of test systems with distinct characteristics. The tuning process of the ensemble model, i.e., determining the ensemble weights, is based on LP and is executed extremely fast (on the order of a few milliseconds). Therefore, its portion in to the overall computation time of the model is negligible. Also, the individual WPPI models within the ensemble structure are independent and can be trained in parallel. As a result, the total computation time of the proposed framework is governed by the individual WPPI model within the ensemble model with the longest training time.

A novel straightforward bi-layer optimization approach is designed for model tuning. It adaptively adjusts the contribution of each individual WPPI model within the EPE to obtain the best prediction results for any given test system. The proposed approach yields WPPIs with maximum sharpness while meeting the SCL requirement as well as maximum symmetricity around the deterministic WPP, reducing the RR standard deviation and the likelihood of high RR values. The effectiveness of the proposed EWPPI framework is verified through simulations and comparisons using three real-world datasets.

This paper is focused on 30-min and 1-hour ahead prediction, however, as a future research direction, the proposed framework can be further expanded for the augmentation of the prediction horizons, which could be achieved by incorporating numerical weather prediction (NWP) data as additional inputs to the proposed framework. This expansion would enable the framework to harness finer-grained meteorological information, enhancing its capacity to anticipate wind variations and resulting in more accurate and robust predictions. In addition, the applicability of the proposed framework extends beyond WPP, making it compelling to explore its adaptation for forecasting other uncertain parameters within power systems such as demand load, solar generation, and electricity price. By leveraging the flexible and straightforward framework proposed in this paper, researchers can construct adaptable methodologies that improve the resilience and efficiency of power system operations in the face of multifaceted uncertainties.

REFERENCES

[1] V. Singh, T. Moger, and D. Jena, "Uncertainty handling techniques in power systems: a critical review," *Electric Power Systems Research*, vol. 203, p. 107633, Feb. 2022.
[2] Y. Zhang, J. Wang, and X. Wang, "Review on probabilistic forecasting of wind power generation," *Renewable and Sustainable Energy Reviews*, vol. 32, pp. 255-270, Apr. 2014.
[3] Z. Meng, Y. Guo, W. Tang *et al.*, "Nonparametric multivariate probability density forecast in smart grids with deep learning," *IEEE Transactions on Power Systems*, vol. 38, no. 5, pp. 4900-4915, Sept. 2023.
[4] J. Wang, T. Niu, H. Lu *et al.*, "A novel framework of reservoir computing for deterministic and probabilistic wind power forecasting," *IEEE Transactions on Sustainable Energy*, vol. 11, no. 1, pp. 337-349, Jan. 2020.
[5] R. J. Bessa, V. Miranda, A. Botterud *et al.*, "Time-adaptive quantile-copula for wind power probabilistic forecasting," *Renewable Energy*, vol. 40, no. 1, pp. 29-39, Apr. 2012.
[6] Y. Shi and N. Chen, "Conditional kernel density estimation considering autocorrelation for renewable energy probabilistic modeling," *IEEE Transactions on Power Systems*, vol. 36, no. 4, pp. 2957-2965, Jul. 2021.
[7] C. Zhao, C. Wan, and Y. Song, "An adaptive bilevel programming model for nonparametric prediction intervals of wind power generation," *IEEE Transactions on Power Systems*, vol. 35, no. 1, pp. 424-439, Jan. 2020.
[8] H. Quan, D. Srinivasan, and A. Khosravi, "Short-term load and wind power forecasting using neural network-based prediction intervals," *IEEE Transactions on Neural Networks and Learning Systems*, vol. 25, no. 2, pp. 303-315, Feb. 2014.
[9] W. Zou, C. Li, and P. Chen, "An inter type-2 FCR algorithm based T-S fuzzy model for short-term wind power interval prediction," *IEEE Transactions on Industrial Informatics*, vol. 15, no. 9, pp. 4934-4943, Sept. 2019.
[10] Z. Shi, H. Liang, and V. Dinavahi, "Direct interval forecast of uncertain wind power based on recurrent neural networks," in *Proceedings of 2019 IEEE PES General Meeting (PESGM)*, Atlanta, USA, Aug. 2019, pp. 1-7.
[11] A. Kavousi-Fard, A. Khosravi, and S. Nahavandi, "A new fuzzy-based combined prediction interval for wind power forecasting," *IEEE Transactions on Power Systems*, vol. 31, no. 1, pp. 18-26, Jan. 2016.
[12] C. Wan, Z. Xu, P. Pinson *et al.*, "Optimal prediction intervals of wind power generation," *IEEE Transactions on Power Systems*, vol. 29, no. 3, pp. 1166-1174, May 2014.
[13] G. Zhang, Y. Wu, K. P. Wong *et al.*, "An advanced approach for construction of optimal wind power prediction intervals," *IEEE Transactions on Power Systems*, vol. 30, no. 5, pp. 2706-2715, Sept. 2015.
[14] C. Wan, Z. Xu, and P. Pinson, "Direct interval forecasting of wind power," *IEEE Transactions on Power Systems*, vol. 28, no. 4, pp. 4877-4878, Nov. 2013.
[15] A. Khosravi, S. Nahavandi, and D. Creighton, "Prediction intervals for short-term wind farm power generation forecasts," *IEEE Transactions on Sustainable Energy*, vol. 4, no. 3, pp. 602-610, Jul. 2013.
[16] F. Liu, Q. Tao, D. Yang *et al.*, "Bidirectional gated recurrent unit-based lower upper bound estimation method for wind power interval prediction," *IEEE Transactions on Artificial Intelligence*, vol. 3, no. 3, pp. 461-469, Jun. 2022.
[17] N. Safari, S. M. Mazhari, and C. Y. Chung, "Very short-term wind power prediction interval framework via bi-level optimization and novel convex cost function," *IEEE Transactions on Power Systems*, vol. 34, no. 2, pp. 1289-1300, Mar. 2019.
[18] C. Wan, J. Wang, J. Lin *et al.*, "Nonparametric prediction intervals of wind power via linear programming," *IEEE Transactions on Power Systems*, vol. 33, no. 1, pp. 1074-1076, Jan. 2018.
[19] C. Wan, J. Lin, J. Wang *et al.*, "Direct quantile regression for nonparametric probabilistic forecasting of wind power generation," *IEEE Transactions on Power Systems*, vol. 32, no. 4, pp. 2767-2778, Jul. 2017.
[20] C. Wan, J. Lin, Y. Song *et al.*, "Probabilistic forecasting of photovoltaic generation: an efficient statistical approach," *IEEE Transactions on Power Systems*, vol. 32, no. 3, pp. 2471-2472, May 2017.
[21] C. Zhao, C. Wan, and Y. Song, "Cost-oriented prediction intervals: on bridging the gap between forecasting and decision," *IEEE Transactions on Power Systems*, vol. 37, no. 4, pp. 3048-3062, Jul. 2022.
[22] C. Zhao, C. Wan, and Y. Song, "Operating reserve quantification using prediction intervals of wind power: an integrated probabilistic forecasting and decision methodology," *IEEE Transactions on Power Systems*, vol. 36, no. 4, pp. 3701-3714, Jul. 2021.
[23] D. Lew, G. Brinkman, E. Ibanez *et al.*, *Eastern Wind Integration and Transmission Study*. Golden: National Renewable Energy Laboratory, 2011.
[24] D. A. Halamay, T. K. A. Brekken, A. Simmons *et al.*, "Reserve requirement impacts of large-scale integration of wind, solar, and ocean wave power generation," *IEEE Transactions on Sustainable Energy*, vol. 2, no. 3, pp. 321-328, Jul. 2011.
[25] E. Hale and E. Zhou, "Absorbing the sun: operational practices and balancing reserves in Florida's municipal utilities," *Nat. Renew. Energy Lab. (NREL)*, Golden, USA, Tech. Rep., Jul. 2021.
[26] M. Milligan, P. Donohoo, D. Lew *et al.*, "Operating reserves and wind

power integration: an international comparison," *Nat. Renew. Energy Lab. (NREL)*, Golden, USA, Tech. Rep. NREL/CP-5500-49019, Oct. 2010.

[27] Alberta Electric System Operator (AESO). (2019, Dec.). Current and historical market data and reports. [Online]. Available: https://www.aeso.ca/market/market-and-system-reporting/data-requests/

[28] Sotavento. (2018, Mar.). Historical wind farm data. [Online]. Available: https://www.sotaventogalicia.com/en/realtime-data/historical

[29] G. James, D. Witten, T. Hastie *et al*., *An Introduction to Statistical Learning with Applications in R*. New York: Springer, 2021.

Hamid Rezaie received the M. Sc. degree in electrical power engineering from Amirkabir University of Technology, Tehran, Iran, in 2017, and the Ph. D. degree in electrical power engineering from the University of Saskatchewan, Saskatoon, Canada, in 2022. He currently works as a Power System Engineer in Grid Operations Support at SaskPower, Regina, Canada. His research interests include power system operation, planning, and uncertainty modeling, prediction models, and artificial intelligence applications.

Cheuk Hei Chung was the Program Leader of the Sustainable Energy and Electricity Awareness and Partnership (SEEAP) Program with the University of Saskatchewan, Saskatoon, Canada, and SaskPower, Regina, Canada. Currently, he is pursuing the B. Sc. degree in Department of Human Biology, University of Toronto, Ontario, Canada. His research interests include clean energy and carbon neutrality.

Nima Safari received the B.Sc. (hons.) degree from K. N. Toosi University of Technology, Tehran, Iran, in 2012, the M. Sc. degree from Tehran Polytechnic University, Tehran, Iran, in 2014, and the Ph.D. degree in electrical engineering from the University of Saskatchewan, Saskatoon, Canada, in 2018. Currently, he is a Grid Analytics Engineer at Alberta Electric System Operator (AESO), Alberta, Canada. His research interests include the application of optimization and machine learning algorithms to integrate large-scale renewable energy generation into power systems.